International Journal of Pharmaceutics 364 (2008) 1–8

Contents lists available at ScienceDirect

International Journal of Pharmaceutics

journal homepage: www.elsevier.com/locate/ijpharm

Kinetic study on hemipenta hydrate risedronate monosodium in batch crystallization by cooling mode

Thi Nhat Phuong Nguyen, Kwang-Joo Kim*

Crystallization Process & Engineering Laboratory, Department of Chemical Engineering, Hanbat National University, Yuseong, Daejeon 305-719, South Korea

ARTICLE INFO

Article history:
Received 3 February 2008
Received in revised form 29 May 2008
Accepted 30 May 2008
Available online 5 June 2008

Keywords:
Hydrate formation
Kinetics
Crystallization
Risedronate

ABSTRACT

The crystallization kinetics of hemipenta hydrate risedronate monosodium (RS) were investigated in cooling mode. The solubility, induction time, mechanism of nucleation and crystal growth in the crystallization of hemipenta hydrate RS in water as a solvent were determined by the in situ measurement using focused beam reflectance measurement (FBRM). The relationship between induction time and the supersaturation was obtained for understanding mechanism of nucleation. The nucleation mechanism including homogeneous and heterogeneous nucleation was grasped with respect to the supersaturation. From the results of nucleation experiments, the interfacial tension of hemipenta hydrate RS was determined. Furthermore, the kinetics of crystal growth was also obtained. The crystal growth of hemipenta hydrate RS was controlled by the combination of one and two-dimensional growth mechanisms.

1. Introduction

Crystallization is one of the most powerful methods for separation and purification in chemical, pharmaceutical and food industries. In the pharmaceutical field, polymorphism, hydrate and solvate forms can perform different physical properties which are closely connected with the bioavailability, bioactivity, compactibility, dissolution, shelf-life and stability of drug substances. Therefore, understanding and controlling hydrate forms are very important for the first consideration to achieve the desired efficacy and to offer the ability to cure diseases on pharmaceutical compounds.

Bisphosphonates such as 3-pyridyl-1-hydro-cyethylidene-1,1-bisphosphonic acid (risedronate) have been used for the treatment of diseases of bone and calcium metabolism. These diseases include osteoporosis, hyperparathyroidism, hypercalcemia of malignancy, osteolytic bone metastases, myositis ossificans progressive, calcinosis universalis, arthritis, neuritis, bursitis, tendonitis and other inflammatory conditions (Cazer et al., 2002). It is known in the literature that risedronate monosodium has an anhydrous form and three hydrate forms including mono, hemipenta and penta hydrates which have not only different morphologies but also various physical properties. In crystallization process, various hydrates containing either stoichiometric or nonstoichiometric amounts of water could be crystallized from the aqueous solution. By adjusting the degree of supersaturation, crystallization mode and operating crystallization conditions, mono, hemipenta and penta hydrates were selectively crystallized (Cazer et al., 2002; Aronhime et al., 2003; Richter and Jirman, 2004, 2005; Godlewski, 2006). Among them, hemipenta hydrate is the most thermodynamically stable form under the typical processing conditions (Cazer et al., 2002) and can be obtained by cooling the aqueous solution to the suitable temperature. However, the kinetics of hydrate formation is still complicated and has never been studied.

To understand the mechanism of the formation of various hydrates, it is necessary to study the kinetics of crystallization. In general, the kinetics of crystallization is determined by measuring the nucleation rate and the growth rate which are the functions of supersaturation. The kinetic study using batch cooling crystallization was based on the analysis of crystal size distribution obtained by FBRM technique (Wang et al., 2006; Dang et al., 2007; Nasser et al., 2008). The best fit of measured data with the various expressions correlating with different nucleation and growth mechanism can identify the kinetics of crystallization (Nasser et al., 2008). Indirect technique to understand nucleation and growth kinetics involves the measurement of induction time concerned with the measurement of solution conductivity, intensity of transmitted light, turbidity, ultrasonic velocity, and focused beam reflectance measurement (FBRM). Many reported works used the dependence of the induction time on the supersaturation to determine the nucleation and growth mechanisms of organic and inorganic

* Corresponding author. Tel.: +82 42 821 1527; fax: +82 42 821 1593.
E-mail address: kjkim@hanbat.ac.kr (K.-J. Kim).

0378-5173/$ – see front matter © 2008 Elsevier B.V. All rights reserved.
doi:10.1016/j.ijpharm.2008.05.037

material (Lee et al., 1976; Mahajan and Kirwan, 1994; Hendriksen and Grant, 1995; Kuldipkumar et al., 2007).

In this paper, the kinetics of hemipenta hydrate RS in crystallization by cooling mode was investigated. The in situ technique by using FBRM was used to determine induction time and growth rate of crystallization. Solubilities of mono and hemipenta RS were also measured. The effect of supersaturation on the nucleation mechanism and growth rate was studied.

2. Materials and methods

2.1. Materials

In this study, mono and hemipenta hydrate of RS (99 mol%, supplied by Dea He Chemical Co., Ltd.) was used as material. RS was identified accurately by XRD, HPLC and DSC before and after experiments. Pure water treated by two-time distillation was used as solvent.

2.2. Experimental method

2.2.1. Measurement of solubility

Solubility of mono and hemipenta hydrate of RS was measured by the isothermal method using the FBRM technique (Kim and Kim, 2007). The schematic diagram of experimental apparatus for solubility measurement used in this study was similar to that shown in Fig. 1. The weight of materials was determined by a Mettler Toledo AB204-S balance with an accuracy of ±0.0001 g. 150 g water used as solvent was placed in a jacket vessel 300 ml covered by the silicon sheet and set with condenser to avoid the evaporation of solvent, and thermostated by the thermostatic bath (JEIO TECH, HTRC-30) with programmable PID controller. A digital thermometer was used to detect and control the internal temperature of the solution with circulating medium within an accuracy of ±0.1 °C.

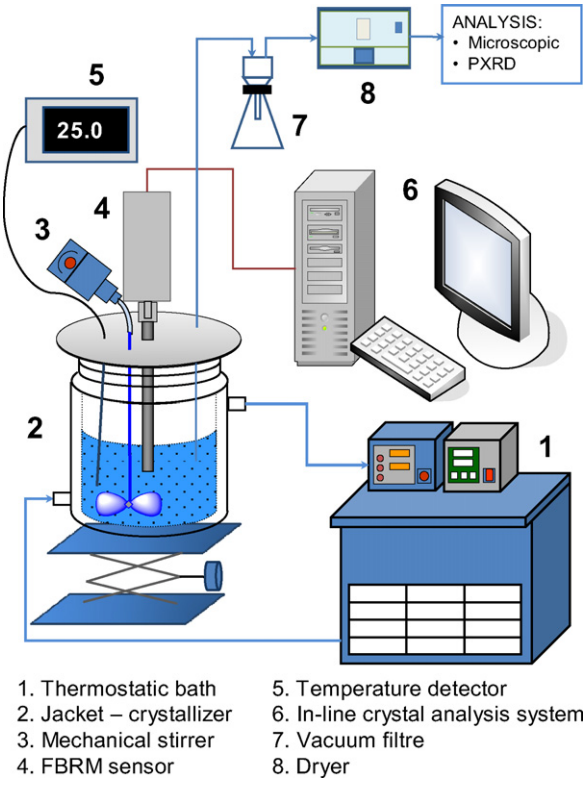

Fig. 1. The schematic diagram for experimental apparatus.

The mixture of solute and solvent was mixed by the mechanical stirrer using a three-blade propeller at 400 rpm speed at constant temperature. The FBRM probe (MODEL M400L-HC-K, Lasen Tech.) which was connected with the in-line analysis system was set up to be settled down in the solution to detect the absence of particles throughout the number of particles recorded in real time. Solute was added one after the other until no particle could be dissolved. Solute of 0.001 g per solvent of 100 g was added every 40 min. The solubility of the solute at given temperature was calculated from the weight of dissolved solute and solvent. The temperature was set in the range from 0 to 99 °C. Some of the experiments were conducted in triplicate to check the reproducibility. The solubility for a given temperature was reproducible within 0.001 g of solute/100 g of solution. Thus accuracy for solubility measurement is in the range of 99.95–99.99%.

2.2.2. Kinetic measurement

The kinetic study was carried out in crystallization by the in situ measurement using FBRM. Experiments with various initial solution concentrations from 0.08 to 0.13 g anhydrous/g water by cooling mode were carried out. The apparatus of experiment setup is shown in Fig. 1. The known amount of monohydrate solid was dissolved in fit-quantity water at 10 °C above the saturation temperature in the 300 ml-jacket vessel. The saturation temperature was determined by the solubility curve for the known solution concentration. After the clear solution was obtained, the supersaturation was generated by cooling the solution from the initial temperature to 25 °C at cooling rate of 5 °C/min. The crystallization temperature was constantly maintained at 25 °C after linear cooling. The experiment data were recorded at intervals of 10 s. The solid product was isolated by vacuum-micro filtration, washed using ethanol as a washing solvent, and dried in the dryer at 50 °C. Then it was identified by optical microscopic and X-ray diffraction (XRD) analysis, which was carried out by RIGAKU Power Diffractometer Model D/Max 2500H with Cu Kα1 radiation (40 kV, 100 mA) at scan speed of 10 deg/min and scan step of 0.05 deg.

3. Results and discussions

3.1. Solubility and the crystallization of hemipenta hydrate risedronate monosodium

Solubility is a very important thermodynamic parameter to determine the crystallization mode, supersaturation, phase diagram and yields. In addition, it can also affect the kinetic of crystallization, the particle size and shape, which are controlled by the supersaturation. Hence, it is necessary to build up the solubility curve of RS. In this study, solubility of hemipenta and monohydrate was determined in the range of 0–99 °C. The solubility data of hemipenta and monohydrate were listed in Table 1

Table 1
Solubility (c^*) data of hemipenta hydrate and monohydrate RS in water

Hemipenta hydrate				Monohydrate			
T (°C)	c^* (g/g)	T (°C)	c^* (g/g)	T (°C)	c^* (g/g)	T (°C)	c^* (g/g)
15.0	0.0379	60.0	0.1105	15.0	0.0440	60.0	0.0923
20.0	0.0434	65.4	0.1201	20.0	0.0544	65.0	0.0990
25.0	0.0494	70.0	0.1357	25.0	0.0588	70.0	0.1055
30.3	0.0579	75.0	0.1403	30.0	0.0610	76.0	0.1188
35.2	0.0651	80.0	0.1500	35.0	0.0671	82.2	0.1246
40.0	0.0720	86.3	0.1619	40.0	0.0723	85.0	0.1274
44.6	0.0795	92.4	0.1749	46.0	0.0778	92.3	0.1332
50.0	0.0930	99.0	0.1801	50.0	0.0811	98.5	0.1351
54.6	0.1033			55.0	0.0863		

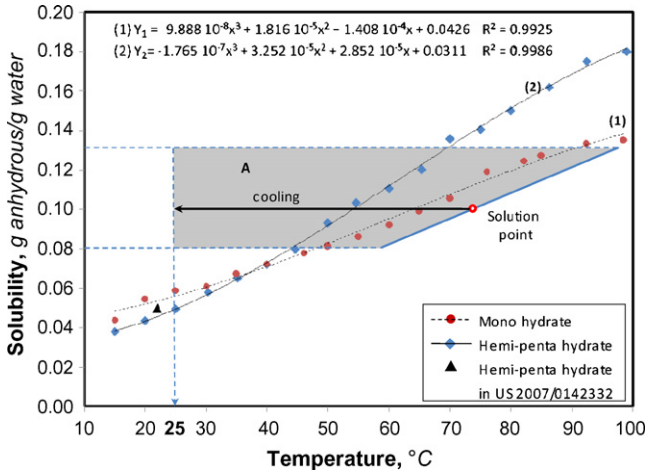

Fig. 2. The solubility of hemipenta and monohydrate RS in water.

and plotted in Fig. 2, in which the solubility of hydrates were expressed as mass of the anhydrous RS per mass of solvent. The previous work presented that the solubility of hemipenta hydrate in water was found to be 0.0497 g/g at 22 °C (Richter et al., 2007). As can be seen in Fig. 2, it is similar to the data measured in this study.

As shown in this figure, the solubility of hemipenta and monohydrates increases with increasing the temperature. Since the solubility depends strongly on the temperature, cooling mode is desirable for crystallization of RS. Furthermore, the solubility curve is divided into two zones: at above 40 °C, the solubility of hemipenta hydrate is higher than that of monohydrate, while at below 40 °C, lower than that. This temperature was consistent with the previous report which found that monohydrate could transform to hemipenta hydrate form in the suspension of monohydrate in water at room temperature and 37 °C (Redman-Furey et al., 2004). For crystallization of hemipenta RS, the experiments were carried out in the shadow zone in Fig. 2, in which only hemipenta RS was formed. The experimental conditions are summarized in Table 2. In this study, as high supersaturation was generated due to the high cooling rate, monohydrate form was not found during the crystallization.

To ensure the selectivity of the hemipenta hydrate, the area of experiments for kinetic study of hemipenta hydrate RS crystallization from monohydrate RS in cooling mode was estimated. XRD patterns of the products were taken using powder X-ray diffraction (PXRD). Fig. 3 shows the XRD patterns of initial raw materials (monohydrate and hemipenta hydrate), hydrate product obtained in crystallization in aqueous solution at 25 °C with various initial concentrations in the shadow area and that of the hemipenta hydrate RS. XRD pattern was identified with the data published previously in the patent (Aronhime et al., 2003). In this figure, the data was collected ranging from 3° to 40° with the characterized peak position at 9.0°, 12.2°, 12.9°, 13.5°, 15.4°, 15.7°, 17.2°, 19.8°, 20.5°, 22.9°, 23.9°, 24.6°, 27.8°, 28.1°, 31.3°, 31.8° ± 0.002° 2-theta. It is obvious that the peaks found in all experiments were well agreed with that of hemipenta hydrate RS. It means that the hemipenta hydrate RS was absolutely crystallized from the aqueous solution at the cooling temperature of 25 °C and at cooling rate of 5 °C/min in the concentration investigated. It is also clear that there is no monohydrate obtained in the hydrate product, which can be explained by the much more stable thermodynamic properties of hemipenta hydrate than that of monohydrate at the conditions investigated. In our experiments, crystallization is generated by high supersaturation at 25 °C. From the solubility curve, mono is first formed, and then hemipenta is formed. Therefore, the late formed RS, hemipenta form is more stable even though solubilities are very near each other. Furthermore, fast cooling mode was also contributed to omit formation of monohydrate as the metastable phase in these experiments.

Table 2
Summarized table of experimental conditions

Initial concentration of solution, C_o (g/g)	Temperature of heated solution (°C)	Final cooling temperature (°C)	Cooling rate (°C/min)
0.08	59	25	5
0.09	67	25	5
0.10	75	25	5
0.11	82	25	5
0.12	90	25	5
0.13	97	25	5

3.2. *In situ monitoring the crystallization by FBRM*

The in situ measurement using FBRM was applied to study the crystallization kinetics of hemipenta hydrate RS in the crystalliza-

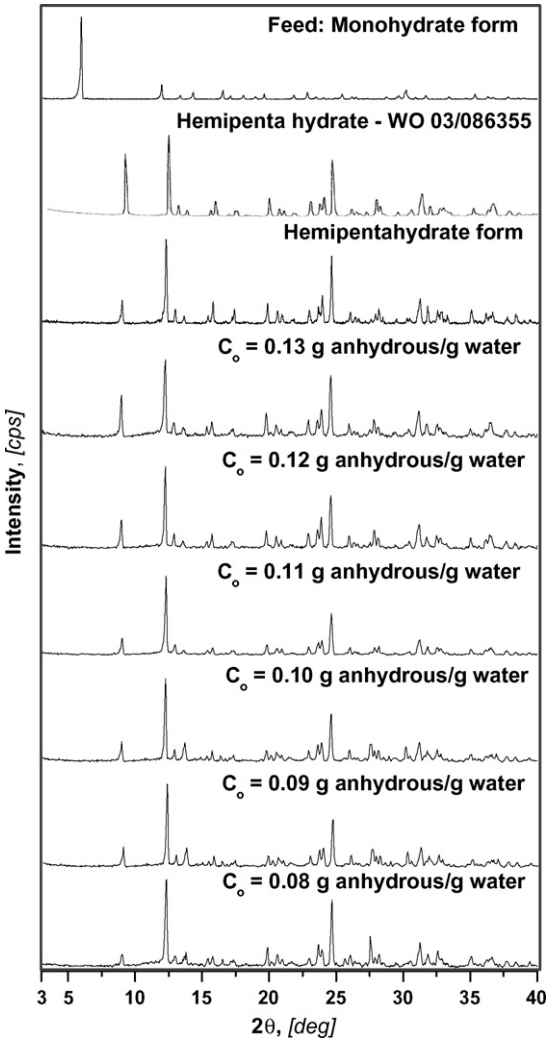

Fig. 3. The XRD patterns of the solid product obtained at various initial concentrations (C_o) in crystallization at 25 °C and that of hemipenta hydrate RS referred in patent WO 03/086355.

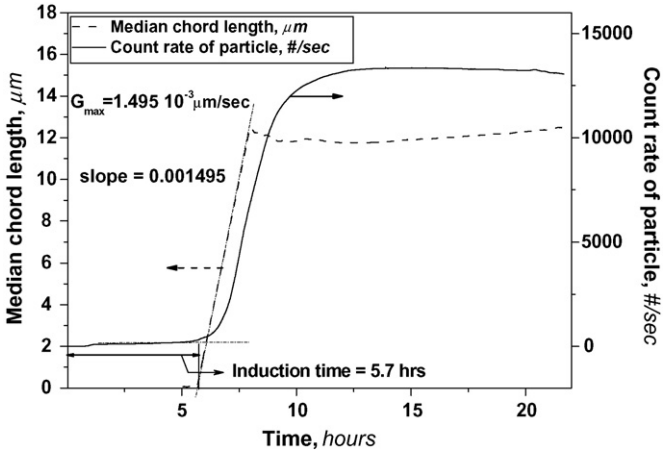

Fig. 4. Typical plot of the total particle number and the mean length chord of particle with elapsed time at temperature of 25 °C and initial solution concentration of 0.10 g/g.

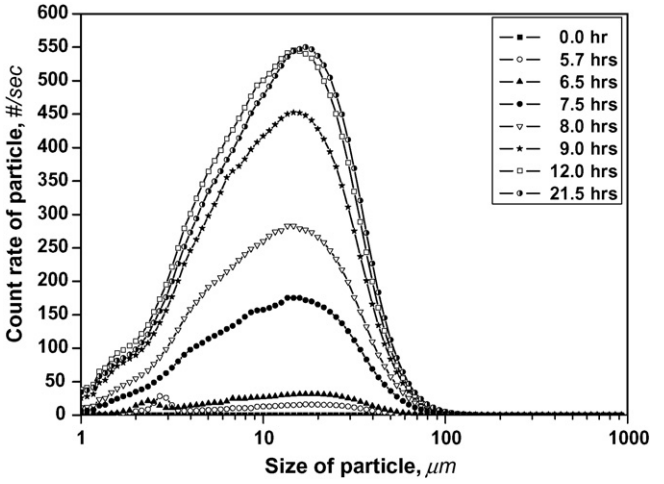

Fig. 5. Variation of particle size distribution during crystallization of hemipenta hydrate RS at initial concentration 0.10 g anhydrous/g water and constant cooling temperature 25 °C.

tion. FBRM provided the trend of the median chord length and the count rate of particle in suspension in real time. Based on this information, the induction time and the crystal growth rate were determined.

The experiments with varied supersaturations were carried out at various initial concentrations obtained by different heating temperatures and cooling to the same cooling temperature of 25 °C with cooling rate of 5 °C. In all initial concentrations, the nucleation did not occur in cooling stage; the induction time for nucleation is needed as the temperature approached and maintained during the crystallization.

Fig. 4 shows the typical data obtained from FBRM which is the plot of count rate and the median chord length with elapsed time at initial solution concentration of 0.10 g/g, cooling temperature of 25 °C and the cooling rate of 5 °C/min. As can be seen, FBRM count was almost equal zero at the beginning, started to increase after approximately 5.7 h because the nucleation occurs and then was constant with time after 12 h. The median chord length also started to increase after 5.7 h owing to nucleation. Because the nucleation occurs during crystal growth, the median size of crystal decreased slightly after about 7 h and then increased due to the crystal growth. From this figure, the induction time and growth rate can be determined. As mentioned in the beginning of this section, nucleation did not occur in the cooling stage. After the temperature approached at 25 °C, the induction time for the nucleation is needed. The cooling rate affects the induction time, which is a driving force for determining the kinetics of nucleation. Generally, the higher induction time leads to the higher supersaturation.

In addition, the crystal size distribution was recorded with temperature every 10 s during the crystallization. Fig. 5 shows the plot of crystal size distribution at various operating time at the same operating condition to Fig. 4. As seen in this figure, the number of crystals was equal zero at the beginning. It started to increase in all ranges of crystal size in 5.7 h due to the nucleation, and then continuously increased with elapsed time with wider distribution because of crystal growth. The number of particles in all sizes was almost constant after 12 h, but distribution of particles moved to larger particle size owing to the ripening until 21.5 h.

It is clear that Figs. 4 and 5 show very useful information to understand the change of crystal size and population of particles during the crystallization including the nucleation and the crystal growth.

3.3. Effect of initial solution concentration

The initial solution concentration is related to the supersaturation, which affects the habit of crystal. Fig. 6 shows the microscopic photos of hemipenta hydrate obtained at various initial concentrations. As the concentration was increased, the crystal size was decreased due to the increase in nucleation rate. The change of crystal size can be expressed more clearly by the distribution of particles at various initial concentrations by FBRM and is showed in Fig. 7. The particle distribution curve shifted to the left side, in which the number of smaller sized particles was increased due to higher nucleation rate. Simultaneously the population of particles also was increased with increasing initial concentration. Furthermore, in Fig. 6, the shape of crystal changed into the needle-like form as the initial concentration increased. Firstly, at the concentration of 0.08 (g anhydrous/g water), particle was found to be hexagonal in shape. Since the concentration increased, the crystal has been elongated due to the faster growth toward one direction. Crystal size and shape is related to the supersaturation. The different initial concentration leads to the different supersaturation even at the same cooling rate. By using the FBRM, crystal size distribution can be compared for effect of concentration. It's clear that the crystal size was decreased as the initial concentration was increased. It means higher concentration results in the higher supersaturation. To understand the importance and influence of supersaturation, nucleation and crystal growth on the properties of crystal, kinetics of nucleation and crystal growth must be grasped.

3.4. Kinetics of crystallization

3.4.1. Nucleation

The time when nuclei are formed, t_n, is defined as the time that elapses from the creation of supersaturation in solution until the critical nuclei form. This lag phase occurs as a consequence of the achievement of steady-state size distribution of the nuclei that are already present in solution or newly formed owing to the supersaturation generated. However, it is impossible to observe the critical nuclei as they form in solution because of the limit of detection technique. These critical nuclei can only be observed after they have grown to a critical size. The induction time, t_{ind}, refers to the time that elapses after is detected and is the experimentally accessible quantity. Therefore, the induction time measurement allows for a connection to be made between nucleation theory and

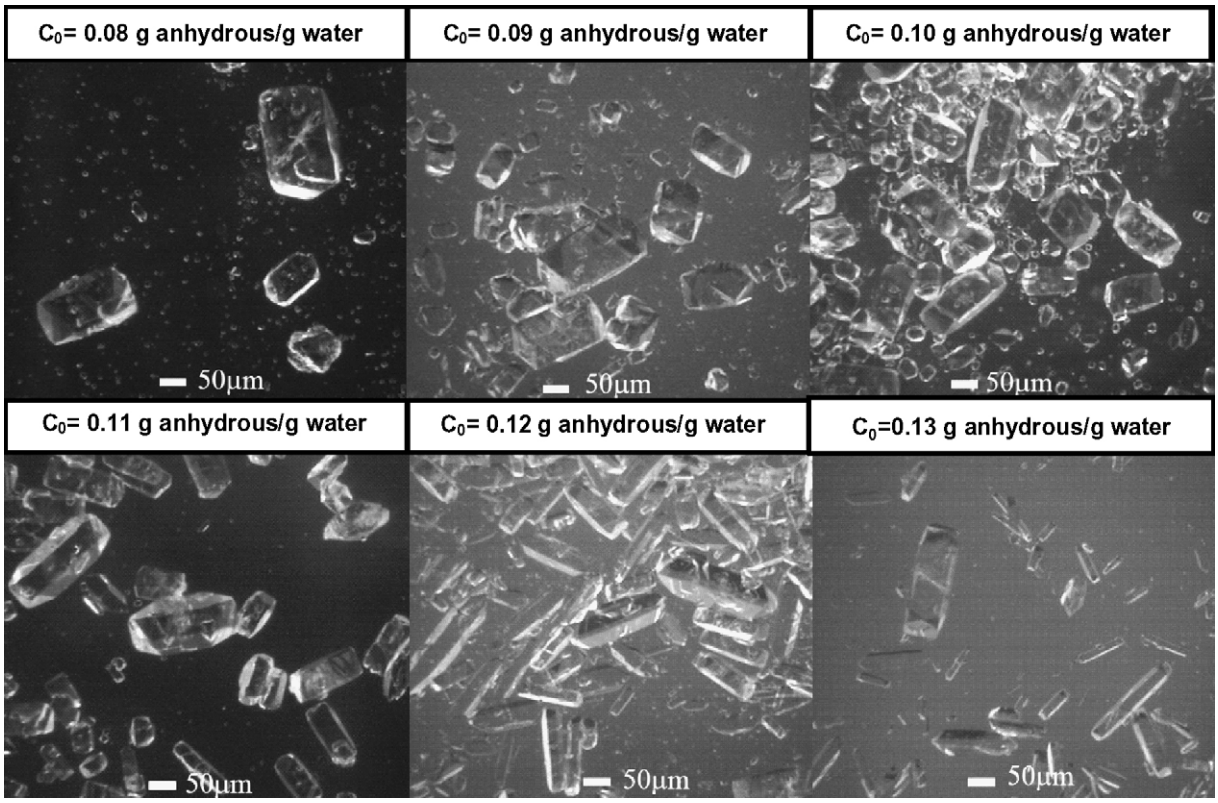

Fig. 6. The influence of initial concentration (C_o) on shape of hemipenta hydrate RS with constant cooling temperature at 25 °C.

experiment investigation. The experimentally determined induction time means the time required for critical nuclei formation and their growth to a detectable size.

In this study, the induction time was detected from the trend for number of particles using FBRM technique. As the solution is clear initially, a minimum or base line in total number of chord particles is recorded. When the nucleation occurs and then nuclei grows until it can be recognized, the total number chord line of particle starts to increase, and the counted number of particles also increases. The point at which the number of particles starts to increase from the basic line determines the induction time.

In Fig. 4, the typical plots of the count rate and the mean length chord of particles were presented against time. It also shows the detection of the induction time. The effect of initial solution concentration on the induction time was investigated. Fig. 8 shows the plot of the count rate of particle with elapsed time at initial solution concentration of 0.08, 0.10, 0,12 and 0.13 g anhydrous/g water. The induction time obtained from Fig. 8 was plotted against the initial concentration in Fig. 9. As expected, the induction time was dramatically decreased with increasing the initial concentration as well as supersaturation because the nucleation increased. To understand the effect of supersaturation on induction time or nucleation, the relationship between induction time and supersaturation was studied.

With the assumption that the t_{ind} is mainly composed of the true nucleation time t_n, which is inversely proportional to the nucleation rate, thus $t_{ind} \propto B^{-1}$. From the conventional nucleation theory, we can get the following equation:

$$\ln t_{ind} = K + \alpha \frac{1}{(\ln S)^2} \quad (1)$$

where $\alpha = 4f_s^3\gamma^3\nu^2/27f_v^2k^3T^3$, k is the Boltzmann constant, T is the absolute temperature, γ is the interfacial free energy, ν is the molecular volume and S is the supersaturation, $S_{max} = c/c^*$, c is the concentration of solution and c^* is the solubility of solute. f_s and f_v are the surface and volume shape factors, respectively and K is the constant.

From Eq. (1), the temperature, degree of supersaturation and interfacial tension are the main factors dominating either nucleation rate or induction time.

Sohnel and Mullin have presented that when the induction time is dominated by the time required for nuclei formation, Eq. (1) is valid (Kuldipkumar et al., 2007). Fig. 10 shows the plot of $\ln t_{ind}$ versus $1/(\ln S_{max})^2$. Instead of S, maximum supersaturation S_{max} is available because supersaturation is varied with time in

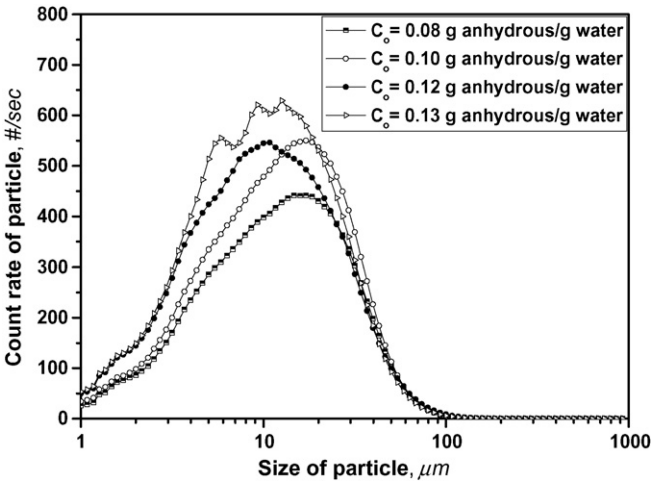

Fig. 7. Particle size distribution at initial solution concentrations (C_o) of 0.08, 0.10, 0.12 and 0.13 g anhydrous/g water at constant cooling temperature 25 °C.

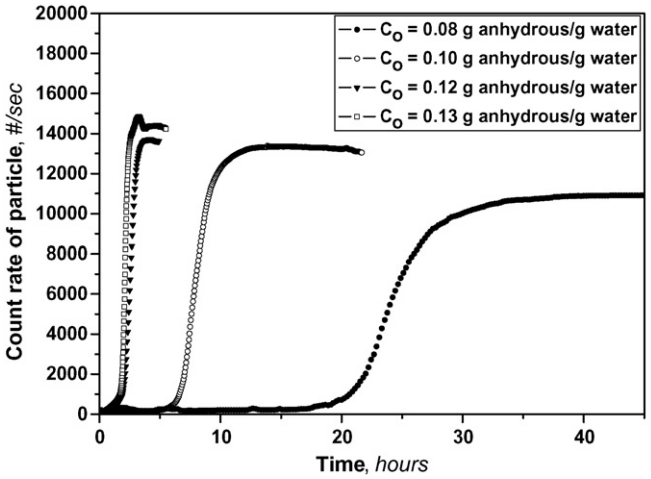

Fig. 8. Total number of particle according to elapsed time at initial solution concentrations (C_o) in crystallization at constant cooling temperature 25 °C.

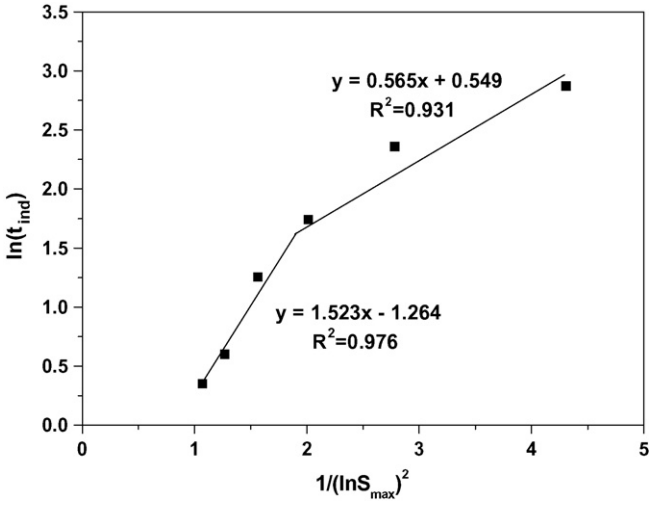

Fig. 10. Plot of $\ln t_{ind}$ versus $(\ln S_{max})^2$ for hemipenta hydrate RS in crystallization with constant cooling temperature 25 °C.

batch crystallization. Maximum supersaturation can be calculated by equation: $S_{max} = c_{max}/c^*$. Here, c_{max} is the concentration of initial concentration and c^* is the solubility at the temperature that nuclei start to be formed. From Fig. 10, it can be seen that the $\ln t_{ind}$ for crystallization of hemipenta hydrate RS was related linearly with $1/(\ln S_{max})^2$ according to Eq. (1). However, there are two regions, divided at S_{max} of about 2.1, including one region of the higher slope at higher maximum supersaturation and the other region of lower slope at lower maximum supersaturation. Similar results have been reported for inorganic salts and organic material (Mullin and Ang, 1976; Wojciechowski and Kibalczyc, 1986; Kuldipkumar et al., 2007). This change has been attributed to the change in nucleation mechanism from homogeneous nucleation at high supersaturation to heterogeneous nucleation at low supersaturation. Generally, the homogeneous nucleation rate has strong dependence on the supersaturation. At high supersaturation, the homogeneous nucleation rate is dominated. Vice versa, at low supersaturation, the heterogeneous nucleation is dominated. In any bulk solution, many dust particles are present that can act as nuclei since they have enough large size. It is impossible to remove all these dust particles, and as result the longer the time lapse without homogeneous nucleation occurring in a supersaturated system, the greater the chance that these dust particles as well as the wall of the crystallization vessel or surface of impeller, which is termed as foreign particle or surface, can act as heteronuclei for the crystals to form. The interplay of homogeneous and heterogeneous nucleation was reflected in Fig. 10.

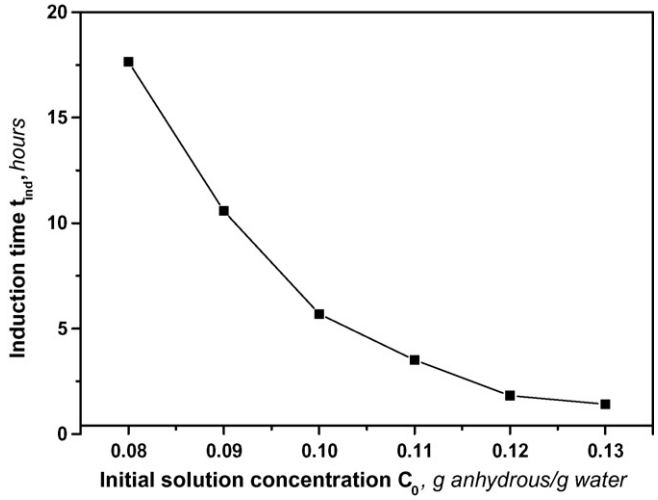

Fig. 9. The plot of induction time against with initial solution concentration (C_o) in crystallization at constant cooling temperature 25 °C.

The proportionality constant (α) in Eq. (1) is composed of the shape factors, the interfacial free energy, molecular volume, and Boltzmann constant. So, the interfacial free energy can be determined from the slope of homogenous nucleation rate if the shape factor and molecular volume were defined. The result of the calculation of shape factors, molecular volume and interfacial free energy was summarized in Table 3. With the assumption that hemipenta hydrate RS has the prism shape having the equilateral hexagonal bottom, the shape factors were estimated to be 26.15 for f_s and 9.24 for f_v. The molecular volume was estimated to be about 3.2×10^{-28} m^3 from the density and molecular weight of the hemipenta hydrate RS. So, from the slope of the line corresponding to homogeneous nucleation, the interfacial free energy (γ) between hemipenta hydrate RS crystal and aqueous crystallization medium was determined to be about 3.26 mJ/m^2. This value agreed well with the values obtained by other authors for different organic material such as acetaminophen (1.73 mJ/m^2) (Hendriksen and Grant, 1995), ure (4.2–8.9 mJ/m^2) (Lee et al., 1976), lovastin (1.45 mJ/m^2) (Mahajan and Kirwan, 1994), asparagines (4.4 mJ/m^2) (Mahajan and Kirwan, 1994) and tolazamide (1.94–2.80 mJ/m^2) (Kuldipkumar et al., 2007). The value of interfacial free energy γ can serve as an indicator of the ability of solute to be crystal-

Table 3
Calculation of the shape factor, molecular volume and interfacial free energy

Side length of equilateral hexagonal bottom, a (μm)	45[a]
Height, h (μm)	196[a]
Area (m^2)	5.3×10^{-8}
Volume (m^3)	8.59×10^{-13}
f_s	26.15
f_v	9.43
Density (g/cm^3)	1.81096
Molecular weight (g)	350.09
Molecular volume (m^3)	3.21×10^{-28}
Interfacial free energy (mJ/m^2)	3.26

[a] The side length and height of crystal was average value which was accurately determined from the microscopic images.

lized from solution spontaneously, the higher its value the more difficult it is for the solute to crystallize. The solid form has the higher interfacial free energy, which results in the more stable form.

3.4.2. Crystal growth

The overall growth rate, G, is defined as the rate of change of a characteristic dimension L of crystal with time, which is often used in batch crystallization process:

$$G = \frac{dL}{dt} \quad (2)$$

By FBRM measurement, the median length chord of particle L was recorded according to time during the crystallization. So, crystal growth rate could be calculated based on the slope of the median size trend along the time axis.

The crystal growth can take place as per various mechanism theories including normal growth, spiral growth, volume diffusion-controlled growth and 2D nucleation-mediated growth mechanism. The dependence of the growth rate on the supersaturation is generally of the form:

$$G = K_G \Delta C_{max}^m \quad (3)$$

where K_G is the growth rate constant and m is the order of crystal growth. As $m = 1$, we have the one-dimension crystal growth which will be controlled by the diffusion following the gradient concentration; $m = 2$: the two-dimension crystal growth which is controlled by the surface-integration from spreading the surface such as spiral growth, volume diffusion-controlled growth and 2D nucleation-mediated growth mechanism; $m = 3$: the third-dimension crystal growth which is controlled by the poly nuclei growth and the growth takes place by the integration of nuclei or small particles due to the interaction and attrition. The exponent plot of measured crystal growth rate obtained by FBRM measurement and supersaturation aids to identify the growth mechanism.

Fig. 11 shows the median size profile with time at 25 °C for various initial concentrations. From this figure, the maximum growth rate values were obtained and plotted with the various initial concentrations in Fig. 12. The growth rate values of hemipenta hydrate RS increased with an increase in initial concentration. An exponential curve fitted to the data points, best describes this trend following the Eq. (3). As is displayed in this figure, the exponent n, the order of crystal growth obtained from the exponent function

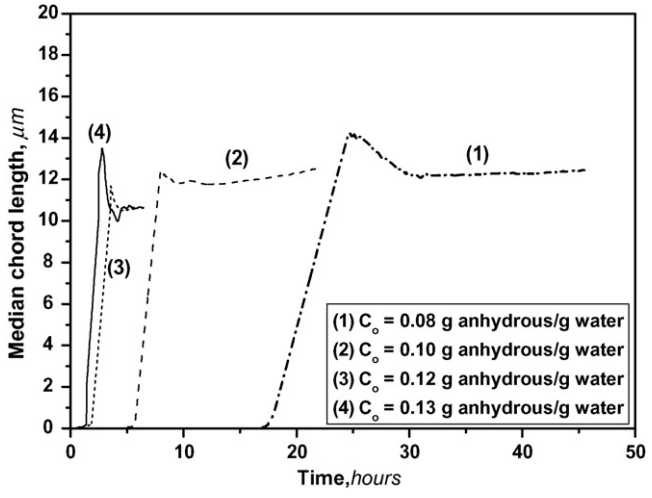

Fig. 11. Variation of median crystal size with elapsed time at constant cooling temperature 25 °C corresponding to various initial solution concentrations (C_o).

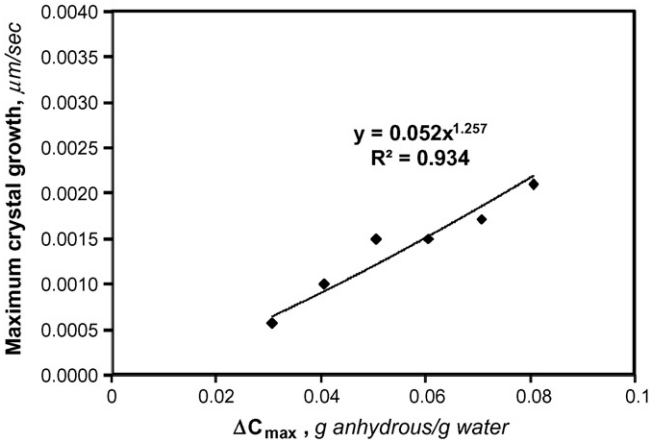

Fig. 12. The plot of maximum crystal growth rate (G_{max}) with maximum allowable supersaturation (ΔC_{max}).

was 1.257. This value is between of the first and the second dimension growth, so it can state that the growth of crystal was controlled by both diffusion and surface-integration.

4. Conclusion

The solubility, induction time, kinetics of nucleation and crystal growth in crystallization by cooling mode of hemipenta hydrate RS were studied. The measured induction time was analyzed according to classical nucleation theory, two different nucleation mechanisms were found to be divided as homogeneous at high supersaturation and heterogeneous at low supersaturation. From the slope of the line corresponding to homogeneous nucleation the crystal/solution interfacial free energy of hemipenta hydrate RS was estimated. It was seen that the crystal growth of hemipenta hydrate RS was controlled by the combination of one and two-dimension growth mechanism.

References

Aronhime, J., Lifshitz-Liron, E., Kovalevski-Ishai, E., 2003. Novel polymorphs and pseudopolymorphs of Risedronate Sodium. PCT WO 03/0086355 A1, 23 October.

Cazer, F.D., Parry, G.E., Billings, D.M, Redman-Furey, N.L., 2002. Selective crystallization of 3-pyridiyl-1-hydroxyethylene-1,1-bisphosphonic acid sodium as the hemipentahydrate or monohydrate. US Patent US006410520B2, 25 June.

Dang, L., Wei, H., Zhu, Z., Wang, J., 2007. The influence of impurities on phosphoric acid hemihydrate crystallization. J. Cryst. Growth 307, 104–111.

Godlewski, J.E., 2006. Process for controlling crystal structure of Risedronate. US Patent US007002014 B2, 21 February.

Hendriksen, B.A., Grant, D.J.W., 1995. The effect of structurally related substances on the nucleation kinetics of paracetamol (acetaminophen). J. Cryst. Growth 156, 252–260.

Kim, D.-Y., Kim, K.-J., 2007. Solubility of cyclotrimethylenetrinitramine (RDX) in binary solvent mixtures. J. Chem. Eng. Data 52, 1946–1949.

Kuldipkumar, A., Kwon, G.S., Zhang, G.G.Z., 2007. Determining the growth mechanism of tolazamide by induction time measurement. J. Cryst. Growth Des. 7, 234–242.

Lee, F.M., Stoops, C.E., Lahti, L.E., 1976. An investigation of nucleation and crystal growth mechanism of urea from water–alcohol solutions. J. Cryst. Growth 32, 363–370.

Mahajan, A.K., Kirwan, D.J., 1994. Nucleation and growth kinetics of biochemicals measured at high supersaturations. J. Cryst. Growth 144, 281–290.

Mullin, J.W., Ang, H.M., 1976. Nucleation characteristics of aqueous nickel ammonium sulphate solutions. Faraday Soc. Discuss. 61, 141–148.

Nasser, W.N.Al., Shaikh, A., Morriss, C., Hounslow, M.J., Salman, A.D., 2008. Determining kinetics of calcium carbonate precipitation by inline technique. Chem. Eng. Sci. 63, 1381–1389.

Redman-Furey, N., Dicks, M., Bigalow-Kern, A., Cambron, R.T., Lubey, G., Lester, C., Vaughn, D., 2004. Structure and analytical characterization of three hydrates and anhydrate form of Risedronate. J. Pharm. Sci. 94, 893–911.

Richter, J., Jirman, J., 2004. A new crystalline form of the sodium salt of 3-pyridiyl-1-hydroxyethylene-1,1-bisphosphonic acid. PCT WO 2004/037252 A1, 6 May.
Richter, J., Jirman, J., 2005. Crystalline form of Risedronate Monosodium. PCT WO 2005/075487 A1, 18 August.
Richter, J., Jirman, J., Petrichova, H., 2007. Amorphous forms of Risedronate Monosodium. US 2007/0142332 A1, 21 June.
Wang, Z., Wang, J., Dang, L., 2006. Nucleation, growth, and solvated behavior of erythromycin as monitored in situ by using FBRM and PVM. Org. Proc. Res. Dev. 10, 450–456.
Wojciechowski, K., Kibalczyc, W., 1986. Light scattering study of KH_2PO_4 and $BaSO_4$ nucleation process. J. Cryst. Growth 76, 379–382.